Since January 2020 Elsevier has created a COVID-19 resource centre with free information in English and Mandarin on the novel coronavirus COVID-19. The COVID-19 resource centre is hosted on Elsevier Connect, the company's public news and information website.

Journal of Inorganic Biochemistry 231 (2022) 111777

Contents lists available at ScienceDirect

Journal of Inorganic Biochemistry

journal homepage: www.elsevier.com/locate/jinorgbio

Inhibition of SARS-CoV-2 replication by zinc gluconate in combination with hinokitiol

Xuan Tao [a,1], Lu Zhang [b,1,1], Liubing Du [c], Kai Lu [a], Zhennan Zhao [a], Yanxuan Xie [a], Xiaobo Li [b], Shuxiang Huang [b], Pei-Hui Wang [d], Ji-An Pan [c], Wei Xia [a,*], Jun Dai [b], Zong-Wan Mao [a,*]

[a] MOE Key Laboratory of Bioinorganic and Synthetic Chemistry, School of Chemistry, Sun Yat-Sen University, Guangzhou 510275, China
[b] Guangzhou Customs District Technology Center, No. 66 Huacheng Avenue, Tianhe district, Guangzhou 510700, China
[c] The Center for Infection and Immunity Study, School of Medicine, Sun Yat-sen University, Guangming Science City, Shenzhen 518107, China
[d] Key Laboratory for Experimental Teratology of Ministry of Education and Advanced Medical Research Institute, Cheeloo College of Medicine, Shandong University, Jinan 250012, China

ARTICLE INFO

Keywords:
SARS-CoV-2
Protease activity
Zinc gluconate
Ionophore
Enzyme inhibition
Protein structure

ABSTRACT

The Severe Acute Respiratory Syndrome Coronavirus 2 (SARS-CoV-2) pandemic is currently the major challenge to global public health. Two proteases, papain-like protease (PLpro) and the 3-chymotrypsin-like protease (3CLpro or Mpro), are indispensable for SARS-CoV-2 replication, making them attractive targets for antiviral therapy development. Here we screened a panel of essential metal ions using a proteolytic assay and identified that zinc gluconate, a widely-used zinc supplement, strongly inhibited the proteolytic activities of the two proteases *in vitro*. Biochemical and crystallographic data reveal that zinc gluconate exhibited the inhibitory function via binding to the protease catalytic site residues. We further show that treatment of zinc gluconate in combination with a small molecule ionophore hinokitiol, could lead to elevated intracellular Zn^{2+} level and thereby significantly impaired the two protease activities *in cellulo*. Particularly, this approach could also be applied to rescue SARS-CoV-2 infected mammalian cells, indicative of potential application to combat coronavirus infections. Our studies provide the direct experimental evidence that elevated intracellular zinc concentration directly inhibits SARS-CoV-2 replication and suggest the potential benefits to use the zinc supplements for coronavirus disease 2019 (COVID-19) treatment.

1. Introduction

The Severe Acute Respiratory Syndrome Coronavirus 2 (SARS-CoV-2) is the cause of the current pandemic of coronavirus disease 2019 (COVID-19) [1]. This worldwide public health crisis has resulted in over 5.6 million deaths globally by the end of January 2022. Similar to the SARS coronavirus (SARS-CoV), SARS-CoV-2 also encoded two essential proteases for processing the polyproteins that are translated from the viral RNA, the papain-like protease (PLpro, encoded within nsp3) and 3-chymotrypsin-like "main" protease (3CLpro or Mpro, encoded by nsp5) [2]. Therefore, the two proteases may serve as promising targets of potential therapeutic reagents. A series of SARS-CoV-2 protease inhibitors have been reported. For example, the approved Human Immunodeficiency Virus (HIV) therapeutics Lopinavir and Ritonavir are being studied in Phase III clinical trials as 3CLpro inhibitors. And several other organic compounds are under consideration in preclinical trials [3–5]. Recently, several metal-based compounds have also been reported to exhibit anti-viral properties, such as Au complexes, bismuth complexes and Re(I) tricarbonyl complexes [6–9]. Despite great effort, there is still no effective antiviral treatment for COVID-19. Due to the rapid spread and increasing number of infected patients worldwide, treatments of cost-effective, safe with minimal side-effects and easy application are urgently warranted.

Structural analysis of SARS-CoV-2 PLpro and 3CLpro reveals that the catalytic center of PLpro consists of a cysteine and a histidine, while the active site of 3CLpro is comprised of a cysteine, a histidine and an aspartic acid. The imidazole group in histidine, the carboxyl group in aspartic acid and especially the thiol group in cysteine are expected to form coordination bonds with transition metal ions. Hence, the proteolytic activities of these two enzymes could be potentially abrogated

* Corresponding author.
E-mail addresses: xiawei5@mail.sysu.edu.cn (W. Xia), cesmzw@mail.sysu.edu.cn (Z.-W. Mao).
[1] These two authors contributed equally to this work.

https://doi.org/10.1016/j.jinorgbio.2022.111777
Received 19 January 2022; Received in revised form 18 February 2022; Accepted 22 February 2022
Available online 1 March 2022

by transition metal ion binding, which further results in the inhibition of SARS-CoV-2 replication as reported previously [10,11]. Accumulating evidence supports for a close relationship between intracellular metal concentration and innate immunity. For example, metal analysis demonstrated that total zinc content was elevated within activated macrophages infected with bacterial or fungal pathogens [12,13]. Recent studies also showed that manganese ion was released from cell organelles and accumulated in the cytosol upon virus infection [14]. The change of intracellular metal concentration endows the host cell with stronger capability to counteract infection.

Herein, we report that the zinc gluconate, a commonly used oral zinc supplement, is a potent inhibitor of the two essential SARS-CoV-2 proteases, PLpro and 3CLpro *in vitro* and *in cellulo*. Co-crystallography of 3CLpro and zinc gluconate showed that free Zn^{2+} bound to the catalytic dyad to impair protease activity. Importantly, treatment of zinc gluconate in combination with hinokitiol ionophore significantly abrogated the protease activities *in cellulo* and inhibited SARS-CoV-2 replication in mammalian cells, indicating that zinc could be a potent inhibitor to suppress SARS-CoV-2 replication (Scheme 1). Inhibition of SARS-CoV-2 replication by zinc-hinokitiol drug combination described here may shed light on development of a safe and easy-to-use approach to treat COVID-19.

2. Results

To investigate whether transition metal ions could impact SARS-CoV-2 polyprotein processing, an *in vitro* proteolytic assay was designed to screen for metal ions against activities of 3CLpro (or PLpro) using a fluorogenic peptide as substrate [15]. As shown in Fig. 1, the presence of divalent transition metal ions Co^{2+}, Ni^{2+}, Cu^{2+} and Zn^{2+} substantially retarded the activities of both PLpro and 3CLpro. For PLpro, Co^{2+}, Ni^{2+}, Cu^{2+} and Zn^{2+} inhibited 54%, 36%, 98% and 98% of the proteolytic activity, respectively (Fig. 1A). Whereas, the proteolytic activity of 3CLpro was abrogated by 36%, 74% and 97.6% in the presence of Co^{2+}, Cu^{2+} and Zn^{2+} (Fig. 1B). In particular, 50 μM Zn^{2+} could completely abolish the activities of both PLpro and 3CLpro. Moreover, fluorescence-based protein thermal shift assays (F-TSA) with different metal ions also demonstrated that Zn^{2+} was the most potent metal ion to decrease the melting temperatures of PLpro and 3CLpro, indicative of destabilization of the two proteases after Zn^{2+}-binding (Fig. 1C and D). The destabilization of the two proteases observed here was probably due to the conformational distortion upon Zn^{2+} binding, since Zn^{2+} is not a physiological ligand for the proteases.

To further investigate Zn^{2+}-binding properties of the two proteases, we examined the Zn^{2+}-binding capability of PLpro and 3CLpro using inductively coupled plasma mass spectrometry (ICP-MS). Apo-PLpro contains 0.85 ± 0.09 molar equivalents (eq.) of Zn^{2+}, which is consistent with the study that PLpro has a conserved zinc-finger site [16]. In contrast, no bound Zn^{2+} content was detected for apo-3CLpro. After incubation with 5 eq. of Zn^{2+}, Zn^{2+}-saturated PLpro had increased binding capacity with 1.90 ± 0.01 eq. of Zn^{2+} per monomer, indicative of an additional Zn^{2+} site. Whereas 3CLpro (monomer) was capable to bind 1.24 ± 0.01 eq. of Zn^{2+} (Fig. S1). In consistent, isothermal titration calorimetry (ITC) experiments also demonstrated that PLpro bound 1.23 ± 0.01 eq. of Zn^{2+} with a dissociation constant value (K_D) of 2.17 ± 0.36 μM, while 3CLpro (monomer) bound 0.79 ± 0.01 eq. of Zn^{2+} with a

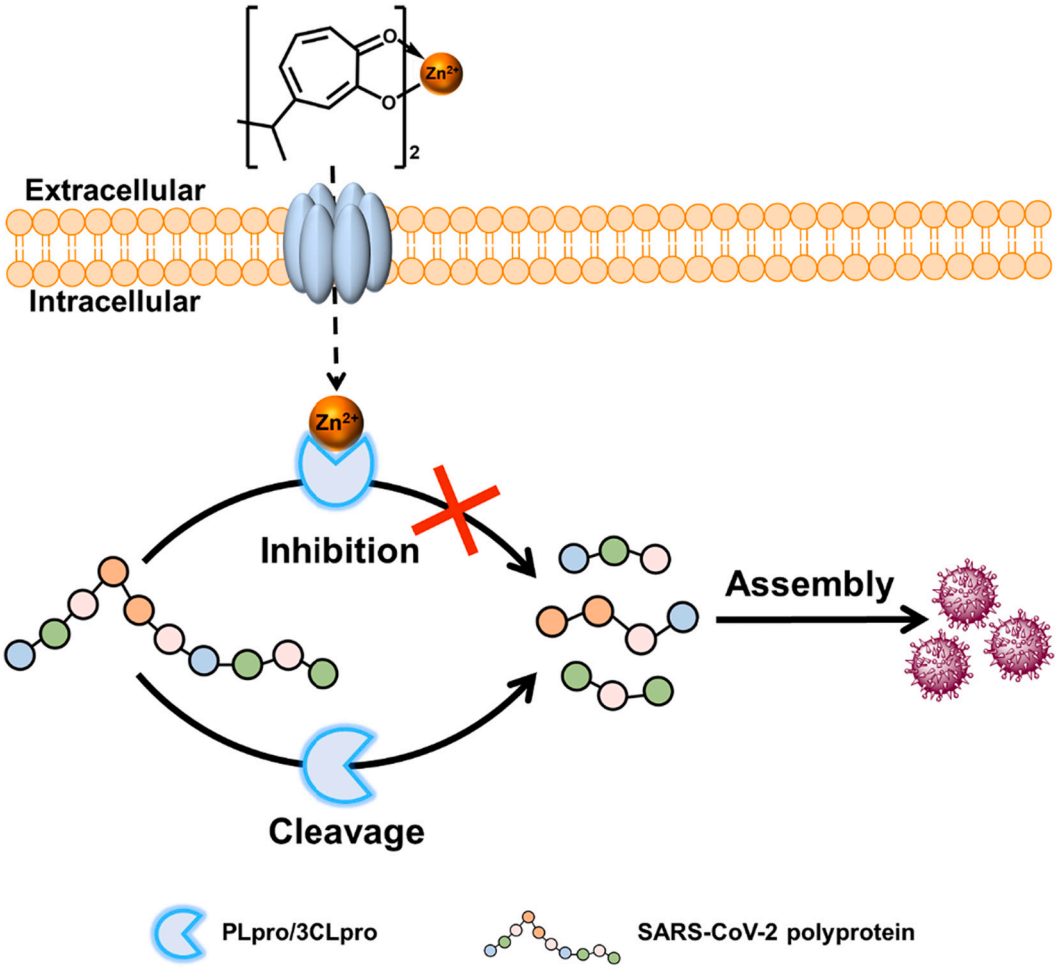

Scheme 1. The mechanism of how a combination treatment of Zn^{2+}-hinokitiol inhibits intracellular SARS-CoV-2 replication.

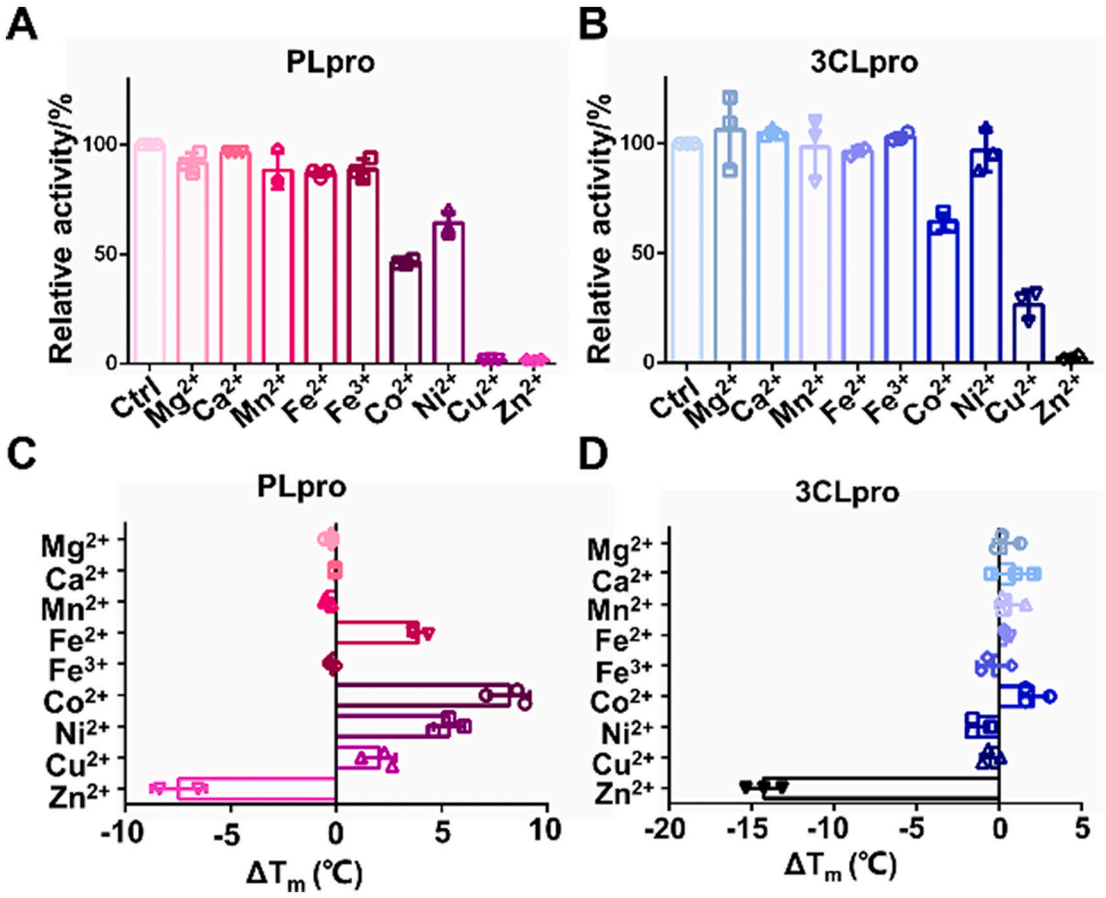

Fig. 1. Identification of inhibitory metal ions for SARS-CoV-2 PLpro and 3CLpro. Bar charts show the relative protease activities of PLpro (A) and 3CLpro (B) after incubation with 50 μM different metal ions, respectively. Fluorescence-based protein thermal shift assays of SARS-CoV-2 PLpro (C) and 3CLpro (D), respectively. Each experiment was performed in triplicates. The data are shown in mean ± sd.

similar K_D value of 4.08 ± 0.66 μM (Fig. S2).

To elucidate the inhibitory activity of Zn^{2+} for PLpro and 3CLpro *in vitro*, the half-maximal inhibitory concentration (IC_{50}) values for Zn^{2+} inhibition were calculated. As shown in Fig. 2A, B, the IC_{50} values of Zn^{2+} for SARS-CoV-2 PLpro and 3CLpro were 0.53 ± 0.04 μM and 0.54 ± 0.04 μM, respectively. The calculated submicromolar IC_{50} values are comparable to reported potent small molecule inhibitors, such as Boceprevir with an IC_{50} value of 4.13 ± 0.61 μM for 3CLpro. In addition, the inhibition of Zn^{2+} to the deubiquitination activity of PLpro was also examined using the ubiquitin-AMC substrate as described previously. And the result revealed that 0.1 μM Zn^{2+} could lead to 95.7% inhibition of PLpro activity (Fig. S3). The Michaelis-Menten saturation curves of PLpro and 3CLpro were also plotted before and after Zn^{2+}-binding. Unexpectedly, the k_{cat} and K_m of the two proteases were both decreased after Zn^{2+}-binding, whereas the k_{cat}/K_m values kept unchanged, implying the Zn^{2+} is an uncompetitive inhibitor for both PLpro and 3CLpro (Fig. S4). Collectively, the results indicated that Zn^{2+} had a high affinity to PLpro and 3CLpro to inhibit their proteolytic activities *in vitro*.

We subsequently try to examine the binding mode of Zn^{2+} to PLpro and 3CLpro by solving the co-crystal structures of Zn^{2+}-bound PLpro and

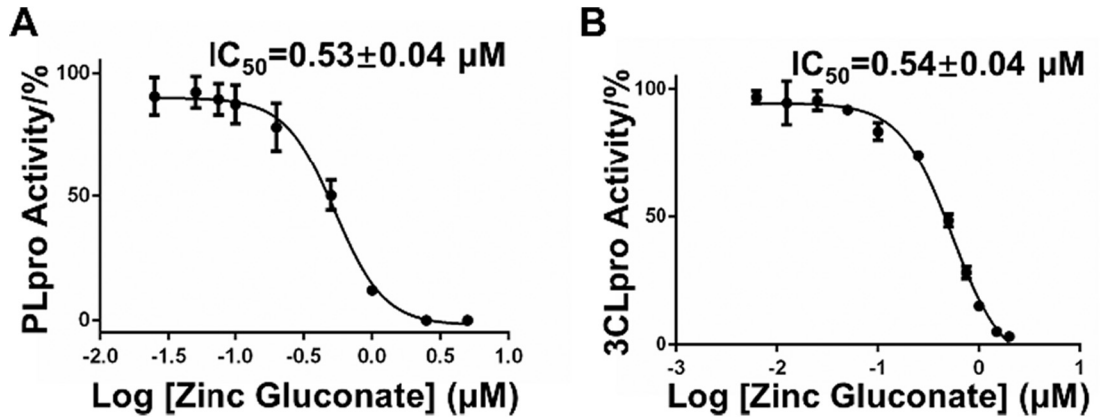

Fig. 2. Inhibition of the protease activities of PLpro (A) and 3CLpro (B) by Zn^{2+} at varying concentrations *in vitro*. Dose-response curves for half-maximum inhibitory concentration (IC_{50}) values were determined by nonlinear regression.

3CLpro. Despite great effort, we were unable to obtain PLpro crystals. However, we found that the catalytic residue mutant PLpro^{C112S} had almost the same Zn^{2+}-binding capacity before and after incubation with excess amount of Zn^{2+}, with 0.85 ± 0.01 and 0.71 ± 0.01 eq. of Zn^{2+} respectively (Fig. S5), indicative of a loss of the additional Zn^{2+}-site besides the zinc-finger. The biochemical experiment results demonstrated that Zn^{2+} bound to the catalytic center to inhibit the proteolytic activity of PLpro.

Fortunately, purified 3CLpro yielded three-dimensional crystals in a reservoir solution containing 15% PEG20000 and 100 mM 2-(N-morpholino)ethanesulfonic acid (MES), pH 6.5. Zn^{2+} was soaked into 3CLpro crystal in reservoir solution that contained 5 mM Tris(2-carboxyethyl)phosphine (TCEP) and 2 mM zinc gluconate for 17 h. Protein crystals were transferred into a cryoprotective solution containing the reservoir solution supplemented with 15–20% glycerol (*v*/v) and flash frozen in liquid nitrogen. The crystals of Zn^{2+}-soaked 3CLpro belong to C2 space group and diffracted to a resolution of 2.45 Å. Initial phases were obtained by molecular replacement with PHASER & Molrep program in CCP4 package using the apo-form SARS-CoV-2 3CLpro (PDB: 6M2Q) as a search model. The final structure model contains one SARS-CoV-2 3CLpro monomer in one asymmetric unit and refined to a R_{work} of 20.1% and R_{free} of 24.2% (Table S2). The overall structure of Zn^{2+}-SARS-CoV-2-3CLpro adopts a typical 3CLpro structure fold with domain I (residues 10–99), II (residues 100–184), III (residues 201–300) and a long loop region (residues 185–200) connecting domain II and III [17]. Structural superimposition reveals that the apo- and Zn^{2+}-SARS- CoV-2-3CLpro structures are quite similar with a backbone r.m.s.d. value of 0.3 Å.

Two sites with redundant electron density in one asymmetric unit were observed, which are assigned as the Zn^{2+} binding sites (Fig. 3A and S6). One site is in the dyad catalytic center (site I), and the other one is located on the surface of the protein structure (site II) (Fig. 3A). The coordination residues of the tetrahedral Zn^{2+} binding site I involve Cys145, His41, His164 and a water molecule (Fig. 3B). Distances between the Zn^{2+} and the sulfur atom in the thiol group of Cys145, the nitrogen atom in the imidazolyl group of His41, the oxygen atom in the main chain of His164 and the water molecule are 2.4 Å, 2.1 Å, 3.9 Å and 4.4 Å, respectively. For the site II, Cys156, Asp153 and Asp155 are involved in binding (Fig. S7). The distances between Zn^{2+} and the sulfur atom in the thiol group of Cys156, the two carbonyl oxygen atoms of Asp153 and the two carbonyl oxygen atoms of Asp155 are 2.6 Å, 2.3 Å, 3.1 Å, 2.7 Å and 3.1 Å, respectively. It is worth noting that ICP-MS results revealed that the 3CLpro (monomer) could only bind 1 molar equivalent of Zn^{2+}. This discrepancy is probably due to the weak association of Zn^{2+} to the highly exposed binding site II during crystal soaking. It is worth noting that the Zn^{2+} coordination sites here are different from recently reported 3CLpro-Zn^{2+} complex structures [18,19]. In the 1.9 Å high-resolution 3CLpro-Zn^{2+}complex structure (PDBID: 7DK1), only one Zn^{2+} site was identified and coordinated with the sidechain of Cys145, His41 and two water molecules. The discrepancy on the Zn^{2+}-binding site is probably due to the different crystal packing.

To exclude the possibility that Zn^{2+} binding to the site II impairs 3CLpro activity, we further constructed a 3CLpro double-mutant 3CLpro$^{D155A/C156S}$ to abolish the binding site II. *In vitro* proteolytic activity assays showed that the activity of 3CLpro$^{D155A/C156S}$ was comparable to wild-type (WT) 3CLpro, suggesting that the overall structure of 3CLpro was not altered by mutations (Fig. S8). However, addition of Zn^{2+} also inhibited the activity of 3CLpro$^{D155A/C156S}$ with a calculated IC_{50} value of 1.54 ± 0.05 μM, which is similar to the value of WT-3CLpro (Fig. S9). Collectively, the results indicated that Zn^{2+} bound to the catalytic site (site I) of 3CLpro and thereby inhibited the proteolytic activity.

Subsequently, we would like to investigate whether Zn^{2+} could impact the proteolytic activities of PLpro and 3CLpro *in cellulo*. Previous study indicated that the free intracellular Zn^{2+} concentration was maintained in nanomolar to picomolar ranges to avoid cytotoxicity, though Zn^{2+} is an essential trace element [20]. Since the K_D values between the two proteases and Zn^{2+} are both in the micromolar range, elevation of the intracellular Zn^{2+} concentration is desired to interfere with the activity of the two proteases *in cellulo*. Hinokitiol (Hino) is a small molecular natural product that was reported to promote mammalian cell uptake of divalent metal ions [21]. Therefore, we tested the possibility to use Hino as an ionophore to elevate intracellular Zn^{2+} concentration. A fluorescent Zn^{2+} indicator 2-[2-[2-[2-[bis(carboxylatomethyl)amino]-5-methoxyphenoxy]ethoxy]-4-(2,7-difluoro-3-oxido-6-oxo-4a,9a-dihydroxanthen-9-yl)anilino]acetate (FluoZin-3) was used to examine the free intracellular Zn^{2+} concentration in cells. As show in Fig. S10, only weak green fluorescence could be detected in resting COS-7 cell, which was in line with that the low concentration of free Zn^{2+} in cytoplasm in most mammalian cell lines. When treated with a combination of 125 μM Hino and 16 μM Zn^{2+} at 37 °C for 30 min, the fluorescent signal enhanced substantially, indicative of elevated intracellular free Zn^{2+} concentration.

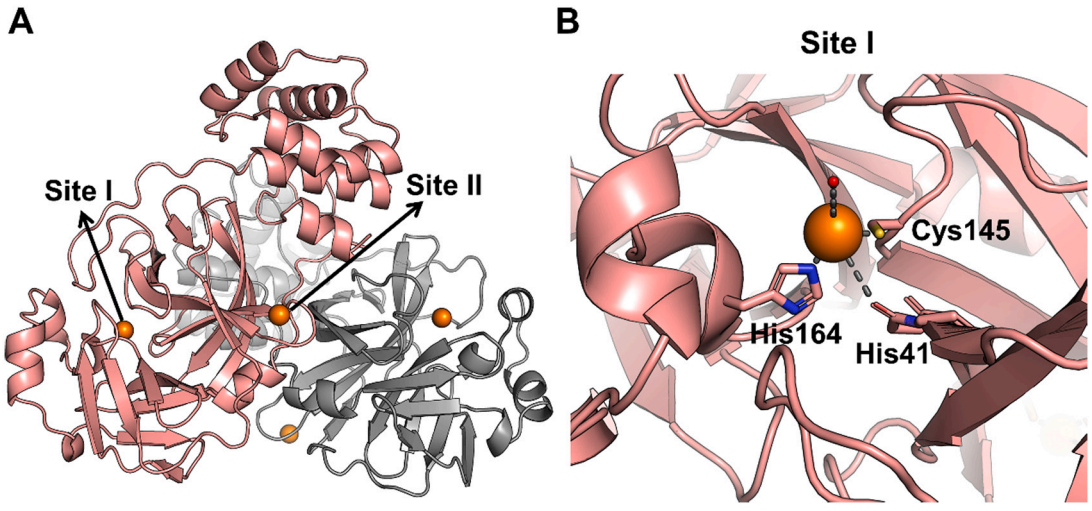

Fig. 3. Crystal structure of the Zn^{2+}-3CLpro. (A) Overall structure of Zn^{2+}-3CLpro homodimer with two potential Zn^{2+}-binding sites. The structure is shown as cartoon model. The two chains are colored in salmon and grey, respectively. Zinc ions are shown in orange spheres. (B) Zn^{2+} binding to the catalytic site of SARS-CoV-2 3CLpro. The ligand residues are shown in sticks model. The coordinated water molecule is shown in red sphere. (For interpretation of the references to colour in this figure legend, the reader is referred to the web version of this article.)

To investigate the proteolytic activity of PLpro and 3CLpro *in cellulo*, we subsequently established a cell-based luciferase reporter assay system (Fig. 4A). In brief, firefly luciferase (Luc) reporter gene is fused with polyubiquitin (UB), which leads to the quick degradation of luciferase in proteasome. A PLpro (or 3CLpro) cleavage site is inserted between Luc and UB. In the presence of PLpro (or 3CLpro), proteolytic cleavage on this site will set free the luciferase and the luciferase activity could be detected. We applied the luciferase assay to examine the proteolytic activities of SARS-CoV-2 PLpro and 3CLpro using nsp2/3 and nsp4/5 peptide as linker between Luc and UB, respectively. As shown in Fig. 4B and C, the luciferase reporter assays results revealed that 32 μM Zn^{2+} in combination with 125 μM Hino could remarkably suppress the *in cellulo* proteolytic activity of SARS-CoV-2 PLpro and 3CLpro by 78% and 75%, respectively. Together, the results demonstrated that the *in cellulo* proteolytic activities of SARS-CoV-2 PLpro and 3CLpro would be inhibited with increasing intracellular Zn^{2+} concentrations.

As we demonstrated that increasing intracellular Zn^{2+} concentration was potent to abrogate PLpro and 3CLpro activities *in cellulo*, we envisioned that this approach would also be applied to inhibit SARS-CoV-2 replication in cell. Therefore, virus infection experiments were performed to test the hypothesis. Previous studies demonstrated that Hino exhibited relative toxicity toward mammalian cell and addition of Mg^{2+} can reduce the cytotoxicity of Hino [22]. To avoid the cytotoxicity effect of Hino, checkerboard method was used to examine the virus inhibition effects of different combinations of Hino and zinc gluconate in the presence of 30 mM $MgCl_2$. In brief, Vero-E6 cells were infected with SARS-CoV-2 at a multiplicity of infection (MOI) of 0.05 with a treatment of different concentrations of zinc gluconate and Hino for 24 h. The nucleus of retained Vero-E6 cells were stained with 4, 6-diamidino-2-phenylindole (DAPI) and virus nucleocapsid (N protein) in the infected cells were blotted and quantified by green immunofluorescence as described in the Supporting Information (Fig. S11). The results are shown in Fig. 5, high dosage of Zn^{2+} and Hino (60 μM) combinations were relatively toxic to Vero-E6 cells, resulting no detectable DAPI signals. However, Zn^{2+} toxicity was significantly attenuated after reducing Hino concentration. Especially, a combination of 30 μM Hino and 125 μM zinc gluconate exhibited no detectable cytotoxicity toward Vero-E6 cell but remarkably inhibited the SARS-CoV-2 replication by 80%. The results clearly indicated that treatment with proper dosage of zinc-Hino mixture could efficiently inhibit intracellular SARS-CoV-2 replication without significant cytotoxicity.

3. Discussions

As the second most abundant element in the cell, Zn^{2+} mainly functions as a cofactor of metalloenzyme [23]. Majority of intracellular zinc presents as protein-bound form and is proven essential for proper folding and activity of various intracellular enzymes and transcription factors. The intracellular concentration of free zinc ion at physiological condition is maintained at a relatively low level, since free zinc ions are relatively toxic and may even trigger apoptosis at elevated concentrations [24]. Furthermore, Zn^{2+} also exerts a critical role in mediating innate immunity. Zinc deficiency could lead to dysfunction of human immune system, such as decreased antibody production, reduced natural killer cell activity and impaired T cell proliferation [25]. Recent studies also reported the relationship between zinc deficiency and SARS-CoV-2 infection. In particular, a very recent observational cohort study with 249 COVID-19 patients demonstrated that serum zinc levels lower

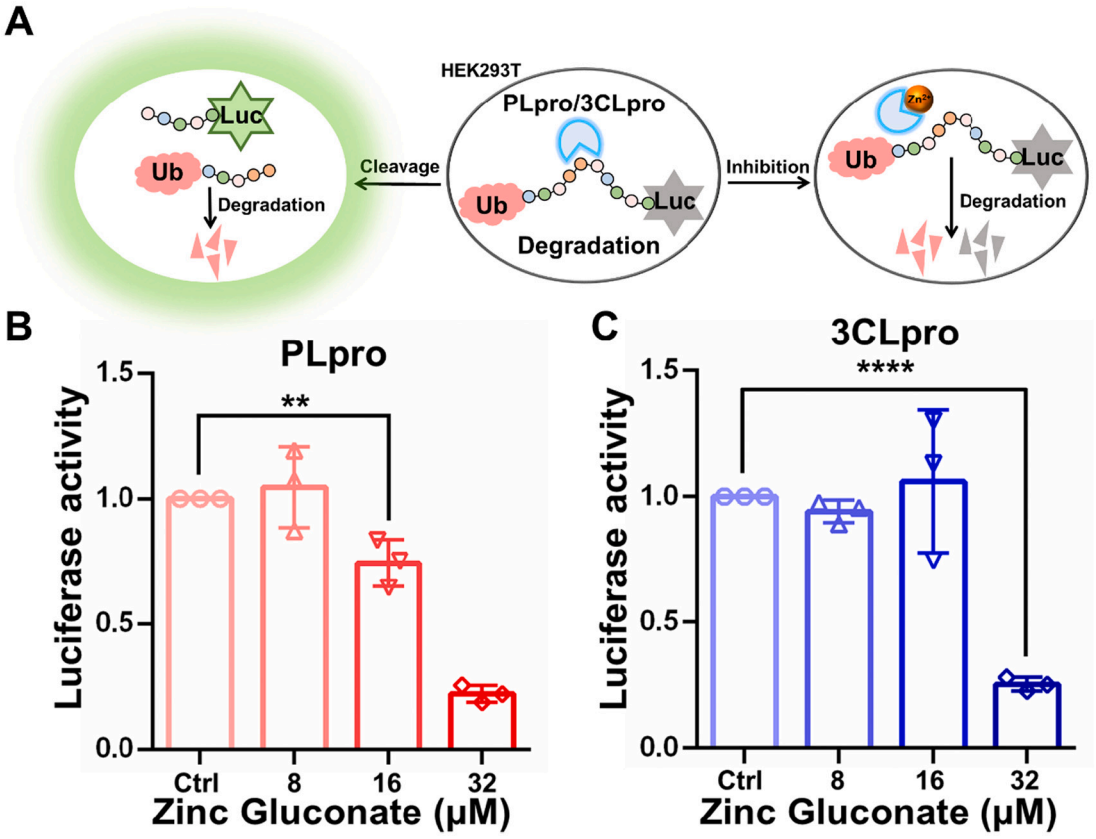

Fig. 4. Increasing intracellular Zn^{2+} concentration with hinokitiol impairs the proteolytic activities of SARS-CoV-2 PLpro and 3CLpro *in cellulo*. (A) Schematic illustration of the proteolytic assays *in cellulo*. The HEK293 cells *co*-express the protease (PLpro or 3CLpro) and polyubiquitin (UB)-fused firefly luciferase (Luc). A protease cleavage site is inserted between Luc and UB. Proteolytic cleavage on this site will set free the luciferase. Bar charts show the relative luciferase activity of cell lysates of HEK293 cells that expressed PLpro (B) or 3CLpro (C) after treatment of 125 μM Hino and varying concentrations of zinc gluconate. Each experiment was performed in triplicates. The data are shown in mean ± sd. ** $p < 0.01$, *** $p < 0.001$, **** $p < 0.0001$.

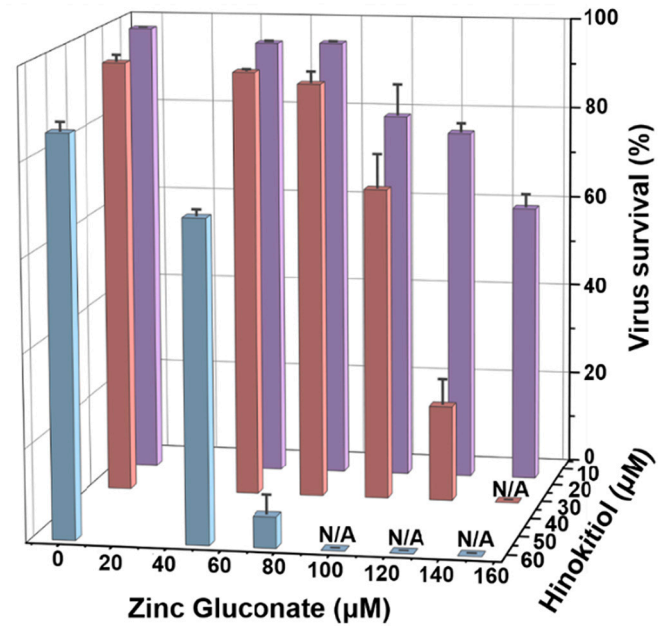

Fig. 5. Inhibition of SARS-CoV-2 replication in Vero-E6 cells by Hino-zinc gluconate. The X-axis represents concentrations of zinc gluconate ranging from 0 to 150 μM, the Y-axis represents concentrations of Hino ranging from 0 to 60 μM, and the Z-axis represents virus survival. N/A indicates that few cells survived after treatment with drugs. Each experiment was repeated in duplicate.

than 50 μg/dL correlated with worse clinical presentation and higher mortality, implying that low zinc levels favor SARS-CoV-2 replication in infected cells [26].

While accumulating clinical data implied the association of the individual zinc status with risk of infection and severe progression of COVID-19, direct research evidence regarding the impact of zinc on SARS-CoV-2 replication is so far missing. Our *in vitro* biochemical and structural studies revealed that Zn^{2+} was a highly potent inhibitor of PLpro and 3CLpro, the two essential proteases of SARS-CoV-2 *in vitro*. Furthermore, cell culture studies demonstrated that increasing cellular Zn^{2+} uptake by ionophore could result in PLpro and 3CLpro dysfunction *in cellulo*. More importantly, enhanced Zn^{2+} importation with proper combination of Hino and zinc gluconate could efficiently inhibit SARS-CoV-2 replication in Vero-E6 cells without significant cellular toxicity. Our findings provide the direct experimental evidence that SARS-CoV-2 infected cells could be rescued by increasing of intracellular free Zn^{2+} concentration.

According to the calculated K_D values between Zn^{2+} and proteases *in vitro*, the intracellular free Zn^{2+} concentrations in our experimental condition should reach micromolar level. It is significantly higher than the reported eukaryotic intracellular free Zn^{2+} concentration in the resting state, which is in the nanomolar to picomolar ranges [20]. Therefore, the ionophore Hino is applied together with zinc gluconate to increase intracellular zinc level. The results implied that mammalian cells could tolerate relatively increased intracellular free Zn^{2+} concentrations. Indeed, it has been reported that the intracellular concentrations of free Zn^{2+} could also dramatically increased in many cells in response to various stimuli. For example, it is reported that cell surface Fcε receptor I activation could directly induce a release of Zn^{2+} from endoplasmic reticulum (ER) to increase intracellular free Zn^{2+} concentration, which is called zinc wave [27]. In addition, free Zn^{2+} could also be released into cytosol from Zn^{2+}-bound metallothionein in response to cellular redox signals [28,29]. Also, it should be noted that high intracellular concentrations would be toxic to mammalian cells, leading to excess reactive oxygen species (ROS) production or even apoptosis. Our study here provides the proof-of-concept that increasing intracellular free zinc concentration could be a potential approach to treat SARS-CoV-2 infection. It is worth noting that a recent study also demonstrated that the natural ionophore quercetin could increase the antiviral potency of Zn^{2+} [19]. However, how to preciously control the intracellular free Zn^{2+} concentration to allow efficient inhibition of viral replication but minimal cytotoxicity warrants further investigation.

In summary, we demonstrated that Zn^{2+} could inhibit the proteolytic activities of SARS-CoV-2 proteases, PLpro and 3CLpro *in vitro*. Crystal structure of Zn^{2+}-bound form 3CLpro showed that Zn^{2+} bound to the catalytic site of 3CLpro and abrogated the proteolytic activity. *In cellulo* proteolytic assay and intracellular virus infection results further indicated that elevated intracellular free Zn^{2+} concentration had significant impacts on SARS-CoV-2 replication in mammalian cells. Our findings not only provide the direct evidence that zinc inhibits SARS-CoV-2 replication in mammalian cells, but also suggest the potential benefits of zinc supplementation in the treatment of COVID-19.

4. Materials and methods

4.1. Protein purification

SARS-CoV-2 PLpro and 3CLpro were expressed and purified as described in supporting information. Protein purity was at least 95% determined by SDS-PAGE.

4.2. In vitro proteolytic activity assays

The detailed procedures of proteolytic assays were described in supporting information. In brief, two fluorogenic peptide substrates Dabcyl-FRLKGGAPIKG(Edans)V and MCA-AVLQSGFR-Lys(Dnp)-Lys-NH_2 were used to measure the proteolytic activities of PLpro and 3CLpro, respectively. The concentrations of PLpro and 3CLpro were 1 μM and 0.5 μM. The initial reaction rates and substrate concentrations were fitted to Michaelis-Menten curve using Graphpad software to obtain V_{max} and K_{cat} values.

4.3. SARS-CoV-2 3CLpro protein crystallization and structure determination

For SARS-CoV-2 3CLpro protein crystallization, 200 nL 3CLpro with concentration of 10.81 mg/mL were mixed with 200 nL reservoir solution consisting of 15% PEG 20000 and 100 mM MES, pH 6.5. Crystals were obtained by hanging drop diffusion at 20°C. The Zn^{2+}-bound 3CLpro crystals were obtained by soaking 3CLpro crystals with 2 mM zinc gluconate for 17 h. Protein crystals were subsequently transferred into a cryoprotective solution containing the reservoir solution supplemented with 25% glycerol (*v*/v) and flash frozen in liquid nitrogen. X-ray diffraction data were collected at the beamline 08ID-1 of Canadian Macromolecular Crystallography Facility (CMCF). Crystallographic data reduction and scaling were processed using XDS and Aimless, respectively. The structures were solved by PHASER & Molrep with CCP4 program and the SARS-CoV-2 3CLpro structure (PDB code 6M2Q) was used as a searching model. Subsequent model building and refinement were carried out in CCP4 and Refmac.2 Crystallographic data statistics are summarized in Table S2.

4.4. In cellulo proteolytic activity assay

The construction of in cellulo 3CLpro/PLpro proteolytic activity reporters (UB-CS-Luc) is described in another manuscript (in preparation). In brief, the reporter gene, firefly luciferase (Luc) is fused with polyubiquitin (UB) which leads to the quick degradation of luciferase in proteasome. A PLpro/3CL protease cleavage site was inserted between Luc and UB. The protein sequence for nsp2/3 cleavage site was FTLKGG↓APTKV and for nsp4/5 cleavage site was TSAVLQ↓SGFRK. The cleavage on this site by PLpro/3CLpro set free the luciferase, the activity

of which could be detected using luciferase activity assay. HEK293T cells were co-transfected with the plasmid encoding PLpro (or 3CLpro), the corresponding UB-CS-Luc reporter gene and the pRL-TK (Renilla luciferase expression plasmid) as an internal control. 24 h post-transfection, the cells were treated with or without 125 μM hinokitiol, 30 mM $MgCl_2$ and various concentrations of zinc gluconate (0–32 μM). After 24 h treatment, the cells were collected and subjected to dual-luciferase reporter assays (Dual-Glo® Luciferase Assay System) following the manufacturer's instruction and the luciferase activities were quantified on Synergy H1 Hybrid Multi-Mode Reader (BIOTEK). Each experiment was performed in triplicate.

4.5. Antiviral activity of zinc gluconate

To evaluate the antiviral efficacy of zinc gluconate, Vero-E6 cells were cultured overnight in 96-well cell-culture plate with a density of 2×10^4 cells/well. Cells were pre-treated with the different concentrations of the indicated zinc gluconate (0–150 μM)-hinokitiol (0–60 μM)-$MgCl_2$ (30 mM) for 1 h. The SARS-CoV-2 virus (MOI of 0.05) was subsequently added to allow infection for 1 h. Virus-drug mixtures were then replaced with fresh medium that only contains zinc gluconate-hinokitiol-$MgCl_2$. After 24 h, the plate was fixed with 4% paraformaldehyde (PFA). The SARS-CoV-2 nucleocapsid protein (N protein) in infected cell was detected with a polyclonal rabbit antibody against SARS-CoV-2-N protein followed by a goat-anti rabbit IgG antibody (Alexa Fluor® 488, ab150077). Cell nuclei were labelled with the DAPI nucleic acid stain. The fluorescence images were acquired with a Celigo Imaging Cytometer.

Data availability

Structure of Zn^{2+}-bound 3CLpro has been deposited at the RCSB Protein Data Bank (www.rcsb.org) with a PDB code of 7D64.

Author contributions

X.T., K.L., W.X. and Z.-W.M conceived the project and designed the experiments. X.T., K.L., Z.Z., Y.X. and P.-H.W. carried out the protein purification and *in vitro* proteolytic assays. L.D. carried out *in cellulo* inhibition experiment. L.Z., X.L. and S.H. carried out virus inhibition experiments and statistical analyses. X.T., L.Z., L.D., J.-A.P., W.X. and Z.-W.M. wrote and revised the paper. J.-A.P., W.X., J.D. and Z.-W.M. supervised the study. All authors proofread, commented on, and approved the final submitted version of the manuscript.

Declaration of Competing Interest

The authors declare that they have no known competing financial interests or personal relationships that could have appeared to influence the work reported in this paper.

Acknowledgements

This work was supported by the National Natural Science Foundation of China (22077142, 22022706, 21837006, 91953117 and 21877131), Natural Science Foundation of Guangdong Province, China (2019A1515011156), the Ministry of Education of China (IRT-17R111) and the Fundamental Research Funds for the Central Universities.

Appendix A. Supplementary data

Supplementary data to this article can be found online at https://doi.org/10.1016/j.jinorgbio.2022.111777.

References

[1] P. Zhou, X.L. Yang, X.G. Wang, B. Hu, L. Zhang, W. Zhang, H.R. Si, Y. Zhu, B. Li, C. L. Huang, H.D. Chen, J. Chen, Y. Luo, H. Guo, R.D. Jiang, M.Q. Liu, Y. Chen, X. R. Shen, X. Wang, X.S. Zheng, K. Zhao, Q.J. Chen, F. Deng, L.L. Liu, B. Yan, F. X. Zhan, Y.Y. Wang, G.F. Xiao, Z.L. Shi, Nature 579 (2020) 270–273.
[2] N. Verma, J.A. Henderson, J. Shen, J. Am. Chem. Soc. 142 (2020) 21883–21890. American Chemical Society.
[3] R. Hilgenfeld, FEBS J. 281 (2014) 4085–4096.
[4] Z. Jin, X. Du, Y. Xu, Y. Deng, M. Liu, Y. Zhao, B. Zhang, X. Li, L. Zhang, C. Peng, Y. Duan, J. Yu, L. Wang, K. Yang, F. Liu, R. Jiang, X. Yang, T. You, X. Liu, X. Yang, F. Bai, H. Liu, X. Liu, L.W. Guddat, W. Xu, G. Xiao, C. Qin, Z. Shi, H. Jiang, Z. Rao, H. Yang, Nature 582 (2020) 289–293.
[5] L. Zhang, D. Lin, X. Sun, U. Curth, C. Drosten, L. Sauerhering, S. Becker, K. Rox, R. Hilgenfeld, Science 368 (2020) 409–412.
[6] M. Gil-Moles, U. Basu, R. Bussing, H. Hoffmeister, S. Turck, A. Varchmin, I. Ott, Chem. Eur. J. 26 (2020) 15140–15144.
[7] S. Yuan, R. Wang, J.F.-W. Chan, A.J. Zhang, T. Cheng, K.K.-H. Chik, Z.-W. Ye, S. Wang, A.C.-Y. Lee, L. Jin, H. Li, D.-Y. Jin, K.-Y. Yuen, H. Sun, Nat. Microbiol. 5 (2020) 1439–1448.
[8] J. Karges, M. Kalaj, M. Gembicky, S.M. Cohen, Angew Chem Int Ed Engl vol. 60 (2021) 10716–10723. John Wiley and Sons Inc.
[9] X. Tao, L. Zhang, L. Du, R. Liao, H. Cai, K. Lu, Z. Zhao, Y. Xie, P.-H. Wang, J.-A. Pan, Y. Zhang, G. Li, J. Dai, Z.-W. Mao, W. Xia, Chem. Sci. 12 (2021) 14098–14102. The Royal Society of Chemistry.
[10] C. DeLaney, Y. Sheng, D.C. Pectol, E. Vantansever, H. Zhang, N. Bhuvanesh, I. Salas, W.R. Liu, C.F. Fierke, M.Y. Darensbourg, Dalton Trans. 50 (2021) 12226–12233. The Royal Society of Chemistry.
[11] K. Rodriguez, F. Saunier, J. Rigaill, E. Audoux, E. Botelho-Nevers, A. Prier, Y. Dickerscheit, S. Pillet, B. Pozzetto, T. Bourlet, P.O. Verhoeven, J. Trace Elem. Med. Bio. 68 (2021) 126818.
[12] H. Botella, P. Peyron, F. Levillain, R. Poincloux, Y. Poquet, I. Brandli, C. Wang, L. Tailleux, S. Tilleul, G.M. Charriere, S.J. Waddell, M. Foti, G. Lugo-Villarino, Q. Gao, I. Maridonneau-Parini, P.D. Butcher, P.R. Castagnoli, B. Gicquel, C. de Chastellier, O. Neyrolles, Cell Host Microbe 10 (2011) 248–259.
[13] K.S. Vignesh, J.A.L. Figueroa, A. Porollo, J.A. Caruso, G.S. Deepe, Immunity 39 (2013) 697–710.
[14] C.G. Wang, Y.K. Guan, M.Z. Lv, R. Zhang, Z.Y. Guo, X.M. Wei, X.X. Du, J. Yang, T. Li, Y. Wan, X.D. Su, X.J. Huang, Z.F. Jiang, Immunity 48 (2018) 675–687.
[15] Y.-S. Han, G.-G. Chang, C.-G. Juo, H.-J. Lee, S.-H. Yeh, J.T.-A. Hsu, X. Chen, Biochemistry 44 (2005) 10349–10359. American Chemical Society.
[16] K. Ratia, K.S. Saikatendu, B.D. Santarsiero, N. Barretto, S.C. Baker, R.C. Stevens, A. D. Mesecar, Proc. Natl. Acad. Sci. U. S. A. 103 (2006) 5717.
[17] Z. Jin, Y. Zhao, Y. Sun, B. Zhang, H. Wang, Y. Wu, Y. Zhu, C. Zhu, T. Hu, X. Du, Y. Duan, J. Yu, X. Yang, X. Yang, K. Yang, X. Liu, L.W. Guddat, G. Xiao, L. Zhang, H. Yang, Z. Rao, Nat. Struct. Mol. Biol. 27 (2020) 529–532.
[18] D. Grifagni, V. Calderone, S. Giuntini, F. Cantini, M. Fragai, L. Banci, Chem. Commun. 57 (2021) 7910–7913. The Royal Society of Chemistry.
[19] L. Panchariya, W.A. Khan, S. Kuila, K. Sonkar, S. Sahoo, A. Ghoshal, A. Kumar, D. K. Verma, A. Hasan, M.A. Khan, N. Jain, A.K. Mohapatra, S. Das, J.K. Thakur, S. Maiti, R.K. Nanda, R. Halder, S. Sunil, A. Arockiasamy, Chem. Commun. 57 (2021) 10083–10086. The Royal Society of Chemistry.
[20] W. Maret, Metallomics 7 (2015) 202–211.
[21] A.S. Grillo, A.M. SantaMaria, M.D. Kafina, A.G. Cioffi, N.C. Huston, M. Han, Y. A. Seo, Y.Y. Yien, C. Nardone, A.V. Menon, J. Fan, D.C. Svoboda, J.B. Anderson, J. D. Hong, B.G. Nicolau, K. Subedi, A.A. Gewirth, M. Wessling-Resnick, J. Kim, B. H. Paw, M.D. Burke, Science 356 (2017) 608–616.
[22] B.M. Krenn, E. Gaudernak, B. Holzer, K. Lanke, F.J.M. Van Kuppeveld, J. Seipelt, J. Virol. 83 (2009) 58–64. American Society for Microbiology (ASM).
[23] K.J. Waldron, J.C. Rutherford, D. Ford, N.J. Robinson, Nature 460 (2009) 823–830.
[24] A.Q. Truong-Tran, J. Carter, R.E. Ruffin, P.D. Zalewski, Biometals 14 (2001) 315–330.
[25] L. Rink, H. Haase, Trends Immunol. 28 (2007) 1–4.
[26] M. Vogel-Gonzalez, M. Tallo-Parra, V. Herrera-Fernandez, G. Perez-Vilaro, M. Chilton, X. Nogues, S. Gomez-Zorrilla, I. Lopez-Montesinos, I. Arnau-Barres, M. L. Sorli-Redo, J.P. Horcajada, N. Garcia-Giralt, J. Pascual, J. Diez, R. Vicente, R. Guerri-Fernandez, Nutrients 13 (2021) 562.
[27] S. Yamasaki, K. Sakata-Sogawa, A. Hasegawa, T. Suzuki, K. Kabu, E. Sato, T. Kurosaki, S. Yamashita, M. Tokunaga, K. Nishida, T. Hirano, J. Cell Biol. 177 (2007) 637–645.
[28] W. Maret, Antioxid. Redox Signal. 8 (2006) 1419–1441.
[29] A. Krezel, W. Maret, J. Am. Chem. Soc. 129 (2007) 10911–10921.